

A Merger Scenario for the Dynamics of Abell 665¹Percy L. Gómez, John P. Hughes²

Department of Physics and Astronomy, Rutgers The State University of New Jersey,
 136 Frelinghuysen Road, Piscataway NJ 08854-8019
 E-mail: percy@physics.rutgers.edu, jph@physics.rutgers.edu

Mark Birkinshaw

Department of Physics, University of Bristol, Bristol, BS8 1TL, UK
 E-mail: mark.birkinshaw@bristol.ac.uk

ABSTRACT

We present new redshift measurements for 55 galaxies in the vicinity of the rich galaxy cluster Abell 665. When combined with results from the literature, we have good velocity measurements for a sample of 77 confirmed cluster members from which we derive the cluster's redshift $z = 0.1829 \pm 0.0005$ and line-of-sight velocity dispersion $\sigma = 1390^{+120}_{-110} \text{ km s}^{-1}$. Our analysis of the kinematical and spatial data for the subset of galaxies located within the central 750 kpc reveals only subtle evidence for substructure and non-Gaussianity in the velocity distribution. We find that the brightest cluster member is not moving significantly relative to the other galaxies near the center of the cluster. On the other hand, our deep *ROSAT* high resolution image of A665 shows strong evidence for isophotal twisting and centroid variation, thereby confirming previous suggestions of significant substructure in the hot X-ray-emitting intracluster gas. In light of this evident substructure, we have compared the optical velocity data with N-body simulations of head-on cluster mergers. We find that a merger of two similar mass subclusters (mass ratios of 1:1 or 1:2) seen close to the time of core-crossing produces velocity distributions that are consistent with that observed.

Subject headings: galaxies: clusters: individual (Abell 665) — intergalactic medium — X-rays: galaxies

¹Optical observations reported here were obtained at the Multiple Mirror Telescope, a joint facility of the Smithsonian Institution and the University of Arizona.

² Also Service d'Astrophysique, L'Orme des Merisiers, CEA-Saclay, 91191 Gif-sur-Yvette Cedex France

1. INTRODUCTION

The study of galaxy clusters has revealed them as powerful probes of such cosmological quantities as the baryon fraction of the Universe (e.g., White & Fabian 1995), Ω_0 (Richstone et al. 1992), and the Hubble constant H_0 (Gunn 1978; Birkinshaw 1979). However, our knowledge of the physics of galaxy clusters has not yet reached the same level of understanding that we have gained for, arguably, the most important cosmological probe to date, i.e., Cepheid variables, and this remains as one of the most significant limitations in our use of clusters for cosmological studies. For instance, one can compute H_0 by combining measurements of the decrement in the brightness temperature of the cosmic microwave background radiation (CMBR) caused by the inverse Compton scattering of CMBR photons by the hot electrons in the cluster (the Sunyaev-Zel’dovich effect, Sunyaev & Zel’dovich 1972) with spectral and imaging observations of the X-ray emission produced by the same hot gas. This technique requires accurate 3-D models of the properties (temperature, density, metallicity, etc.) of the cluster atmosphere, which in turn demands that the physics and astrophysics of clusters be well understood. However, this understanding presents a problem because even present-day clusters are dynamically young and active, showing evidence for the accretion and merger of other systems. The resulting rich complexity in their internal properties greatly complicates their use for precision cosmology.

Abell 665 was initially classified by Abell (1958) as the richest cluster in his catalog. As such, it has been the subject of considerable study across the wavebands. Evidence for subclustering in the spatial distribution of the galaxies was first presented by Geller & Beers (1982). This was later confirmed through BVR photometry of 178 galaxies by Kaloglyan et al. (1990). The luminosity function has been recently studied by Garilli et al. (1996), Wilson et al. (1997), and Trentham (1998) for comparison with other clusters and in an effort to evaluate models for galaxy evolution.

Despite its richness, only 33 cluster members in A665 have published redshifts (Oegerle et al. 1991, hereafter OHFH). OHFH examined the kinematical properties of these galaxies and found that the velocity distribution was well described by a Gaussian with a relativistically-corrected line-of-sight velocity dispersion of $\sigma = 1201^{+183}_{-126} \text{ km s}^{-1}$. This seemed to indicate a fairly relaxed, but massive cluster. However, these authors did not completely reject the possibility that the cluster could be more complex. They suggested that the observed spatial substructure in the galaxy distribution and the relatively large peculiar velocity ($v_{pec} = 447 \text{ km s}^{-1}$) of the brightest cluster member (BCM) argued for a non-relaxed dynamical state for A665. We will have more to say on this point later.

A665 is also a luminous source of X-ray emission, as its optical richness and high velocity dispersion would suggest. The presence of hot gas in this cluster was demonstrated by early observations performed by the *Einstein Observatory* and the *Ginga* satellite (Birkinshaw, Hughes, & Arnaud 1991; Hughes & Tanaka 1992). These pioneering observations revealed some evidence that the spatial distribution of the X-ray-emitting gas deviated from circular symmetry. Birkinshaw et al. modeled the complex gas distribution and found that a combination of two

isothermal- β models separated by $\sim 3'$ provided a considerably better fit to the data than a single isothermal- β model did. Hughes & Birkinshaw (1996, 2000) have applied this type of modeling in much greater detail to *ROSAT* PSPC data and came to the conclusion that the properties of the X-ray emission required that a major merger was occurring or had occurred recently in this system. Note that Markevitch (1996) also suggested that a recent merger could explain the temperature gradient and asymmetric X-ray emission detected in *ASCA* observations of A665.

Further support for a merger scenario comes from Buote & Tsai’s (1996) study of the X-ray morphologies of a sample of 59 bright X-ray clusters. Their work quantifies cluster substructure by characterizing the X-ray surface brightness in terms of a multipole expansion of the two-dimensional gravitational potential. They detect a tight correlation between specific multipole power ratios that suggests an evolutionary track for clusters (i.e., the location of a cluster in the P_2/P_0 – P_4/P_0 power ratio plane is a function of its dynamical state). Interestingly, Buote & Tsai find that the only cluster in their entire sample that deviates from this correlation is A665. They hypothesized that A665 is undergoing a major merger event and is in a brief period of its evolution when the X-ray emitting hot gas does not follow the dark matter distribution or the gravitational potential.

The goal of this paper is to present new velocity measurements for galaxies in A665 and, by combining them with data from the literature, to study the cluster’s dynamics and to investigate the parameters of the cluster merger that we infer to have taken place recently. In section 2 we describe the acquisition and reduction of new optical and *ROSAT* X-ray data. In the following section we present our analysis of these data. Then in section 4 we present our model for the dynamical state of A665. We summarize our conclusions in section 5. We use $H_0=75 \text{ km s}^{-1} \text{ Mpc}^{-1}$ and $q_0=0.5$ throughout the paper.

2. OBSERVATIONS AND DATA REDUCTION

2.1. Optical

Initially we used a 0.6 m telescope CCD image to identify and measure the positions of a total of 147 objects in the inner $5'.5$ region of A665 to a relative position uncertainty of $0''.5$. Later we obtained rough R band photometry for these objects from images obtained on 31 December 1991 and 6 March 1992 at the Fred L. Whipple Observatory 1.2 m telescope on Mt. Hopkins. At that time, the telescope was equipped with a thick, front-illuminated Loral 2048×2048 CCD with a nominal pixel size of $\sim 0''.32$. Its $\sim 10'$ field-of-view allowed us to mosaic a large area of the cluster by observing the cluster center and four regions offset by $\sim 5'$ to the NW, NE, SW, and SE. Each set of observations consisted of six individual 300 s exposures (with small positional offsets between frames) in order to reduce cosmic-ray contamination and cosmetic defects in the CCD chips. Each image was bias-subtracted and flat-fielded using a dome flat and then a sky flat was constructed from the median combination of all individual frames.

A grayscale plot of the final image is shown in Figure 1. From this image we computed R band magnitudes for the galaxy targets within a fixed $5''$ radius aperture. Short observations of Landolt (1992) standard stars allowed us to reduce our measurements to the Johnson-Kron-Cousins system. To determine the zero point offset we compared our measurements with the magnitudes from a photometric, calibrated sample of galaxies in A665 (Trentham 1998). We find a root-mean-square (rms) dispersion of $m_R \sim 0.13$ in the magnitudes of the 55 galaxies in common between our and Trentham’s sample. We consider this to be the uncertainty in the overall accuracy of our photometry.

Of the 147 potential targets in our sample, we observed a total of 89 objects during seven spectroscopic observing runs at the Multiple Mirror Telescope (MMT). Table 1 lists the combination of spectrographs, gratings, and aperture masks used in these runs. The atmospheric conditions were generally good, except for the March 1990 observing session, which was hampered by bad weather and poor seeing. The first three runs used the faint-object grism spectrograph (FOGS) (Geary, Huchra, & Latham 1986) while the remaining spectra were acquired with the Red Channel spectrograph (Schmidt, Weymann, & Foltz 1989).

Two gratings, one with 400 lines mm^{-1} and the other one with 300 lines mm^{-1} , were used with the FOGS. They offered resolutions of 11\AA and 15\AA over nominal spectral ranges of 4000\AA – 6700\AA and 3800\AA – 7500\AA , respectively. The red channel spectrograph was equipped with a 270 lines mm^{-1} grating that provided a typical spectral resolution of $\sim 11\text{\AA}$ over 3800\AA – 7400\AA (nominal). Note that the exact spectral range depended on the location in the focal plane of the slit for each spectroscopic target. This was because, in order to acquire simultaneous observations of order 10 galaxies per exposure, we used either a movable multislit assembly (labeled “slitlets” in Table 1; Geary et al. 1986) or a set of custom-made aperture plates (Fabricant et al. 1991). The choice of spectroscopic targets for any individual field was constrained by factors associated with laying out the aperture plates or the positions of the slitlets. Nevertheless the large number of aperture plate or slitlet configurations we used (11) resulted in a reasonably uniform sampling of cluster member galaxies.

The total exposure time was 1–2 hrs for each field. These exposure times were built up of individual exposures of 20–30 minutes each in order to avoid excessive contamination by cosmic rays. We traced and extracted sky-subtracted spectra from each individual flat-fielded frame using standard IRAF tasks. The tracing of the spectra had typical rms residuals of ~ 1 pixel. Then the He-Ne-Ar arc lamp spectra (extracted from the 2-D spectral data using the same tracing as for the corresponding object spectrum) were wavelength calibrated by identifying at least 30 spectral lines and fitting their pixel positions against their known laboratory wavelengths with a third order polynomial function. The fits produced solutions with rms residuals of $\sim 1\text{\AA}$ ($\sim 50 \text{ km s}^{-1}$). Subsequently, we co-added the spectra from the individual frames and checked the accuracy of the wavelength solution by measuring the positions of several night sky lines in galaxy spectra that were not sky subtracted. The typical differences between the measured and actual sky line positions were generally $< 1\text{\AA}$ except for the June 1989 and January 1990 observations, which

showed larger offsets ($\sim 20\text{\AA}$). Although we were unable to determine the cause of these large offsets, we were able to correct for both the large and small wavelength offsets by shifting the overall wavelength scale of the data by the average difference of the measured and true wavelengths of the night-sky lines. We verified that the large corrections applied to the January 1990 data were accurate by comparing the velocity of galaxy #7 (see Table 2) from that observing run with a previous one and noting a small velocity difference ($\sim 68\text{ km s}^{-1}$). Moreover, observations of NGC 4486B during the June 1989 and January 1990 runs for calibration purposes resulted in corrected velocities that were in general agreement (within 180 km s^{-1}) with published values (de Vaucoulers et al. 1991).

The galaxy recessional velocities were computed using the IRAF task FXCOR. This task allowed us to cross-correlate the observed spectra (after removal of cosmic rays and any possible emission lines and ignoring spectral regions containing bright night-sky lines) with a high signal-to-noise spectrum of NGC4486B generated for the CfA redshift survey. Table 2 lists the coordinates (in epoch J2000), heliocentric velocities and errors, the Tonry & Davies (1979) ‘R’ parameter (TDR) from the cross-correlation, the R-band magnitude, and comments, as appropriate, for the 147 galaxies in our original sample. In the top part of the table we list the 55 spectroscopic targets that we confidently identify as galaxies, based on a high TDR value (≥ 3.5) and visual inspection of the spectra. The galaxies are ordered by right ascension and numbered sequentially. Each cross-correlation was further inspected and the derived redshifts were confirmed by identifying the locations of prominent absorption line features. The bottom part of the table lists the remaining objects in the original sample, also in right ascension order. Secure identification was not possible for these objects, either because the object was not observed spectroscopically or because its spectrum was insufficient to admit a positive identification (e.g., TDR values < 3.5). The objects in the latter case were generally faint: the median magnitude of the unidentified spectroscopic targets was 19.5, versus a median magnitude of 18.6 for the identified ones. In the bottom part of the table we also indicate possible stars, which we consider to be any unresolved object brighter than the BCM and in fact, two of these appear in the HST Guide Star Catalog. A possible background galaxy is indicated as well.

The velocity errors listed in this table were computed by adding in quadrature the formal uncertainty from the cross-correlation (as output by task FXCOR), with our estimates for the errors from sky-subtraction, arc-lamp wavelength calibration ($\sim 50\text{ km s}^{-1}$), and shift in the absolute wavelength scale from the wavelengths of the night sky lines ($\sim 20\text{ km s}^{-1}$). The errors caused by sky-subtraction were estimated by varying the parameters of the function used to fit the positional variation of the night sky brightness in the cross-dispersion direction. We estimate these errors to be $\sim 45\text{ km s}^{-1}$. Finally, we note that the template galaxy used for the cross-correlation was not completely successful at identifying galaxies with strong Balmer absorption line features. Two of our galaxies (numbered 9 and 11, denoted BLG in Table 2) appeared to show such spectra. We calculated their redshifts manually and estimate a velocity error of 150 km s^{-1} for them.

As an internal check on our velocity measurements, we made repeat observations of five

galaxies during the course of the project. The average difference in the derived velocities is 58 km s^{-1} , well within our quoted errors. And as a final check, we compared our velocities with those published by OFHF for the seven galaxies in common, viz., 1, 2, 12, 34, 42, 46, and 49 (which correspond to galaxies 231, 235, 225, 201, 224, 218, and 234, respectively, in OFHF’s numbering scheme). The average velocity difference is -51.0 km s^{-1} and the rms dispersion is 130 km s^{-1} , which is also within our velocity uncertainty. The largest difference was for galaxy 1, which showed a difference of -324 km s^{-1} ; however, OFHF report the presence of a cosmic ray in their spectrum of this galaxy, which might have affected their estimate of its redshift.

In order to determine how representative of the cluster our final spectroscopic sample is, we compared the radial distributions of the identified galaxies in the top part of Table 2 with all the galaxy candidates in our catalog minus an estimate for the galaxy field population (Trentham 1998). The ratio of the number of identified galaxies to the number of candidate galaxies was computed for three radial bins each $1'2$ (200 kpc) wide centered on the BCM. We obtained values of 0.49, 0.5, and 0.46 for the ratios in the three bins. This distribution is fairly flat, which suggests that there is not a serious radial bias in the final sample of identified cluster galaxies. We also compared the number-magnitude counts of galaxies in the velocity range $50,000\text{--}60,000 \text{ km s}^{-1}$, which are likely cluster members, with the photometric results of Trentham (1998). Our sample of members of A665 is not complete; we have spectroscopically confirmed the membership of only 57% of the expected number of cluster galaxies down to $m_R = 19$ (or 40% of the expected members brighter than $m_R = 20$). Nevertheless the shape of the number-magnitude distribution is quite similar to that of Trentham’s at least down to magnitude 19. Thus although our sample of galaxies is not a complete or well-defined subsample of the full population of cluster members, it appears fairly representative.

2.2. X-ray

Our *ROSAT* high resolution imager (HRI) observation of A665 was carried out in two parts; the first set of observations (rh800774) was done on April 1996 and lasted for a total of 41,224 seconds (live-time corrected) while the second set (rh800900) was performed in May 1997 and contained 57,650 seconds of live-time corrected exposure. These individual observations were summed after verifying that there was no significant offset in their relative pointing directions. Next, we boresight-corrected the absolute positions of the combined data set using two known radio sources (MB20 and MB28 from Moffet & Birkinshaw 1989) that were also X-ray sources. The difference in X-ray and radio source positions were $0''.4$ (right ascension) and $2''.7$ (declination). With these corrections, we estimate that the absolute X-ray positions are accurate to $\lesssim 1''$.

The raw data were block-averaged to produce an image with $8''$ pixels. The total background level was determined by computing the counts from an annular region centered on the cluster with an inner radius of $5'$ and a width of $10'$ avoiding obvious point sources. This yielded a background level of $4.8 \times 10^{-3} \text{ counts s}^{-1} \text{ arcmin}^{-2}$ which is consistent with the range seen in other ROSAT

HRI observations (David et al. 1998). Note that the total number of background subtracted counts within a radius of $5'$ of the peak of X-ray emission ($\alpha_{J2000} = 8^h30^m59.8^s$, $\delta_{J2000} = 65^\circ50'31.3''$) is ~ 17780 . Figure 1 shows an overlay on the R-band image of the X-ray surface brightness contours from the background-subtracted HRI data adaptively-smoothed to an approximate signal-to-noise ratio of 5 which yields a typical smoothing scale of $15''$ within the inner $2.5'$ of the image (see Huang & Sarazin 1996 for a description of the smoothing algorithm).

3. DATA ANALYSIS

3.1. Optical Data Analysis

We assembled a sample of 89 potential cluster members by combining our 55 galaxies with 34 different ones from OHFH. Note that OHFH’s entire sample contained 41 galaxies, but there were seven objects in common with our sample; for these we use our redshift measurements. Cluster membership was determined using an iterative 3σ clipping criteria (Yahil & Vidal 1977). The outlier galaxies were easily identified (after a single iteration): we find the same eight outlier galaxies as OHFH did in their sample as well as four more in our own sample. These latter are flagged in Table 1 as lying in either the foreground or background. We are left with 77 galaxies as cluster members in the total sample. Due to the relatively modest number of galaxies in our sample, we replaced the classical statistical estimators for the mean and dispersion with the more robust biweight estimators (Danese et al. 1980, Beers et al. 1991). The redshift of the cluster from the total sample is $0.18285^{+0.00045}_{-0.00064}$ and the 1-D velocity dispersion is 1390^{+120}_{-110} km s $^{-1}$ (1σ errors). The uncertainties were determined through a bootstrap technique using the ROSTAT software (Beers et al. 1991). Our value of the cluster’s velocity dispersion is consistent with the value derived from the well-known correlation between X-ray temperature kT and velocity dispersion σ . Using an average X-ray temperature for A665 of $kT = 8.3$ keV (Hughes & Tanaka 1992) and the relationship between kT and σ given by Girardi et al. (1996), we estimate $\sigma = 1230$ km s $^{-1}$. Table 3 lists the redshift and 1-D velocity dispersion for the total sample and various subsamples of the cluster galaxies. Since we are especially interested in the dynamics of the galaxies located near the center of the cluster, we concentrate the remainder of our analysis on the 54 galaxies located within $4.5'$ (750 kpc) of the BCM (galaxy #34 in Table 2). Figure 2 shows the velocity histogram for these galaxies.

We applied a number of statistical tests to search for evidence of substructure in the spatial and kinematical distribution of the central galaxies in A665. Our tests find weak evidence for skewness in the velocity distribution. Specifically, using the B1 (D’Agostino 1986) and W (Yahil & Vidal 1977) tests we can reject the Gaussian hypothesis at the 92% confidence level. The B1 test is the usual third moment in the distribution while the W test computes the skewness based on ordered data. Note that the more conservative Asymmetry Index estimator (Bird & Beers 1993), which tests for symmetry by comparing gaps on the left and right side of the ordered velocity data,

yields a significance of $\sim 97\%$ for skewness. The statistical significance of other deviations from Gaussianity (e.g., kurtosis and bimodality) is even smaller. Therefore, the velocity distribution is barely distinguishable from Gaussian in form.

Furthermore there is no evidence for significant substructure in the 2-D spatial distribution of the centrally located galaxies, i.e., we do not detect strong asymmetries or bimodality in the locations of the galaxies.

Finally, we tested for the presence of substructure using 3-D tests that consider both the spatial and kinematical positions of the galaxies. The only test that resulted in even a marginal signal is the Dressler-Schectman test (Dressler & Schectman 1988). This test compares the local mean velocity (v_i) and dispersion (σ_i) for galaxy i (computed in this case from the seven nearest neighbors) with the global mean velocity (v) and dispersion (σ) by calculating the quantity δ_i , where $\delta_i^2 = [(\sqrt{N} + 1)/\sigma^2][(v_i - v)^2 + (\sigma_i - \sigma)^2]$ and $N = 55$ is the number of sample galaxies, and then summing to compute the statistic, $\Delta = \sum \delta_i$. The statistical significance of the value $\Delta = 69.2$ that we calculate for the galaxies in A665 was determined through Monte-Carlo simulations. We find that our observed value of Δ is larger than 95% of the Δ values obtained by random simulations in which the velocities were shuffled while keeping the positions fixed. Figure 3 is a graphical representation of the Dressler-Schectman test, where a circle, whose radius is proportional to the quantity e^{δ_i} , is plotted at the position of each cluster member galaxy. A concentration of large circles in any particular area indicates the presence of galaxies whose kinematical properties differ from the global values. Although no obvious pattern dominates the deviations between the local and global values, the plot shows that most of the galaxies with large delta values (i.e., large circles in Fig. 3) lie close to a line that is perpendicular to the axis of X-ray elongation. These galaxies have local mean velocities that differ from the global mean velocity by as much as 1350 km s^{-1} and signal the presence of non-relaxed groupings of galaxies in the cluster. In the following section we will review what implications can be drawn from these results.

We do not detect any significant peculiar velocity of the BCM with respect to the sample of 54 centrally-located galaxies. In particular we measure a peculiar velocity of $20 \pm 220 \text{ km s}^{-1}$ while OHFH found a velocity of 447 km s^{-1} for the BCM relative to their sample of galaxies, a difference that was statistically significant at the 98% confidence level. Our separate, independent velocity measurements for the BCM are in agreement, so it is the difference in our estimates for the mean recessional speed of the cluster that must be the cause of the discrepancy. As Table 3 shows, the galaxies located close to the center of the cluster (our sample) have a mean velocity that is slightly larger than the mean velocity of the galaxies located in the outer regions of the cluster. Since the mean recessional velocity of the latter sample agrees well with OHFH’s sample, the discrepancy between our results, at least, is explained. The relativistically-corrected velocity difference between the inner and outer samples of galaxies is $580 \pm 290 \text{ km s}^{-1}$, yet another marginal (2σ) indication that the galaxy population in A665 is not fully relaxed. Whether this indicates that there is a radial velocity gradient in the cluster, or a velocity differentiation based on galaxy type awaits improved imaging data and a larger sample of measured redshifts.

Finally, Figure 4 shows a grey scale map of the surface density of central cluster galaxies overlaid with the X-ray surface brightness contours. Two features to note are (1) the offset of the peaks of the X-ray emission and the galaxy density by a small amount $\sim 1'$ (167 kpc) and (2) the NW-SE elongation of the brighter parts of both distributions. The generally good agreement between the spatial distributions of the gas and confirmed cluster member galaxies argues strongly against the possibility that the distorted appearance of the X-ray emission is the result of a superposition of unrelated clusters along the line of sight.

3.2. X-ray Data Analysis

We carried out an elliptical isophotal analysis of A665's X-ray surface brightness using the algorithm developed by Jedrzejewski (1987) as implemented in IRAF (using task ellipse in the stsdas package). The program uses an iterative least-squares technique to model the radially decreasing surface brightness with elliptical isophotes. The centroid (row and column pixel positions), axial ratio, and position angle of the major axis are varied to obtain the best fit. Figure 5 shows the results of these fits to the adaptively-smoothed *ROSAT* HRI data in four panels that present the radial variation from the peak of the X-ray emission ($\alpha_{J2000} = 8^h30^m59.8^s$, $\delta_{J2000} = 65^\circ50'31.3''$) of the axial ratio, position angle (measured positive counter-clockwise from north), and centroid shifts in right ascension and declination.

The errors shown were estimated using a Monte Carlo technique. One hundred simulated images of the cluster were generated by adding Poisson noise to the original adaptively-smoothed X-ray data. Each separate realization was re-smoothed and then run through the ellipse program. The error at each radial point was estimated by computing the rms dispersion of the 100 fitted values obtained from the different realizations. Note that this technique explicitly takes account of the statistical error from Poisson noise as propagated through the ellipse fitting process.

As figure 5 shows, there is significant centroid movement, ellipticity variation, and isophotal twisting. For example, by a radius of 2.5 the centroid of the isophotes has shifted by over $1'$ toward the NW. Note that this shift is larger than the overall smoothing scale within this region ($\sim 15''$) and roughly the same as the direction of elongation of the central part of the galaxy surface density distribution mentioned in the previous section. The shape and orientation of the isophotes are also a function of radius. They are initially fairly elliptical ($\epsilon = 1 - b/a \sim 0.17$) with the major axis aligned slightly toward the NE. Over the next arcminute in radius, the isophotes twist as the position of the major axis rotates by -45° (i.e., toward the west). At this point the major axis points in nearly the same direction as the direction of the centroid shift. The orientation of the isophotes remains nearly constant for the next arcminute or so in radius before continuing to twist further toward the west. Beyond a radius of ~ 2.5 , the signal to noise ratio of the data has become too low to pursue further fits. These results are generally consistent with the substructure detected in the PSPC images of A665 by Hughes & Birkinshaw (2000), which required a number of spatial components, at least two isothermal- β models as well as two ellipsoidal distributions of

hot gas, to explain in detail.

4. DISCUSSION

Based on the results of our optical data alone, we would be hard pressed not to conclude that A665 is a relaxed cluster. The velocity dispersion, although high, is not inconsistent with measurements of other rich clusters (e.g., Zabludoff et al. 1993; Edge & Stewart 1991). We detect only marginal evidence for substructure and non-Gaussianity in the velocity distribution of the cluster members. The BCM appears to be at rest with respect to the gravitational potential, at least as traced by the dense concentration of galaxies near the cluster center. In short, all the tests that we have used on the galaxy data are consistent with a fairly simple, relaxed cluster scenario.

On the other hand, the morphology of the X-ray emitting gas indicates an entirely different situation for the dynamical state of the cluster. The strongly asymmetric distribution of the X-ray emitting gas, the isophotal twisting and centroid variation presented above, and the exceptional nature of A665’s morphology as discussed by Buote and Tsai (1996) all argue strongly against a typical relaxed cluster interpretation. These facts suggest that the hot cluster gas is not in hydrostatic equilibrium with the cluster gravitational potential or, if it is, then the gravitational potential must be strongly asymmetric, clumpy, or highly structured in some way. The possibility of a chance line-of-sight superposition of two isolated, nearly-regular, clusters giving rise to the distorted appearance of A665 can be rejected based on the general agreement between the spatial distribution of cluster member galaxies (with $cz \sim 50000 \text{ km s}^{-1}$) and the X-ray emission (Fig. 4). An alternate scenario that may be consistent with the observations is one in which A665 is undergoing a recent merger and that the inherent complexities in the dynamics of the galaxies are somehow hidden from us. This scenario could naturally account for the X-ray substructure and, depending on the merger epoch and viewing geometry, might be consistent with the spatial and kinematical properties of the galaxies. In the following, we explore this merger hypothesis in more detail.

Numerical simulations (e.g., Evrard 1990; Pearce et al. 1994; Schindler & Müller, 1993; Roettiger et al. 1996) show that during a major merger, the gravitational potential of a cluster is severely disrupted. Shocks heat and compress the gas, eventually redistributing a portion of the energy associated with the merger to the cluster gas. However during the actual merger itself, the gravitational potential evolves too rapidly for the cluster atmosphere to respond on the sound-crossing timescale, and consequently the gas falls out of hydrostatic equilibrium. Shocks, the exchange of gas between the merging components, and the reaction of the gas to the gravitational forces all give rise to structures, elongations, and other asymmetries in the X-ray emission. These processes, we believe, provide a plausible qualitative explanation for the X-ray substructure seen in A665. Yet these simulations also predict the presence of substructure in the spatial and kinematical distributions of the cluster member galaxies. Have we failed to observe these effects in A665 because our galaxy sample is too small, the properties of the merger (epoch

and viewing geometry) are unfavorable (see, for example, Pinkney et al. 1996), or because the underlying premise of a major merger in A665 is just plain wrong?

We decided to test the merger hypothesis by comparing our optical data with the results of N-body simulations of simple head-on cluster mergers. We do not aim for a precise match between the data and simulations (and we do not carry out an exhaustive study); we try only to determine whether this general type of merger can produce the subtle kinematic deviations from an apparently relaxed cluster that we observe. We assume that the galaxies are good probes of the underlying gravitational potential and that light traces mass.

Given the significant distortions in the X-ray emission, we have chosen to focus on major mergers for maximum effect. We tried two general types of merger: one consisting of a merger of equal mass components (1:1) and one with merging components in mass ratio of 1 to 2 (1:2). All simulations were performed using Hernquist’s N-body code (TREECODE, Hernquist 1987). We started with simple, idealized initial conditions. Each of the component subclusters was modeled as an isothermal sphere (King 1966, Binney & Tremaine 1987) characterized by a concentration parameter of 1.08 (so that the tidal radius is ~ 12 times the core radius). The initial core radii were fixed at a value of 250 kpc for the equal mass cluster simulation, while in the 1:2 merger they were 250 kpc (main cluster) and 198 kpc (subcluster). These choices ensured an equal matter density between the merging subclusters and are consistent with values found in the literature (e.g., Mohr et al. 1999). Note that this choice fixed the length scale for the simulations and left, as the single remaining scalable parameter, either the mass per N-body particle or the time step of the simulation. The two subclusters were allowed to merge head-on under the influence of their mutual gravity. At the start the two merging components were separated by 8 Mpc and 6 Mpc for the 1:1 and 1:2 models, respectively, and had initial velocities consistent with their free-fall velocities ($\sim 1000 \text{ km s}^{-1}$). The total number of particles in the computations was 30000, divided appropriately between the two components.

In order to compare to the observed velocity distribution of the galaxies it was necessary to apply a numerical scaling to the velocities of the N-body particles, since the model calculations were done in scale-free coordinates. Fixing the velocity scaling is equivalent to defining the time step of the simulations which in turn determines the masses of the merging components. The other quantities of interest to us for the comparison were the merger epoch and the viewing direction, i.e., the angle between our line-of-sight and the merger axis. We investigated three different viewing angles: 30° , 45° , and 90° (where 0° corresponds to viewing along the merger axis). Only N-body particles within a projected radius of 750 kpc about the center of mass of the system were used in the model velocity distribution. The Kolmorov-Smirnoff (KS) test was used for the comparison.

The results are shown in Figure 6. The two panels show the two different mass ratios used for the initial conditions. In each panel the vertical axis shows the initial mass of the main merging subcluster while the horizontal axis shows the time since core-crossing. The different symbols

indicate the different viewing directions assumed. Only models with a (2-sided) KS probability for rejection of 90% or less (i.e., those with a maximum difference between the model and the data distributions of $\lesssim 0.076$) are plotted. Overall 8700 possible models as a function of epoch (from -6 Gyr to 5 Gyr with a typical timestep of ~ 0.3 Gyr) and initial main subcluster mass (from $0.7 \times 10^{15} M_{\odot}$ to $1.5 \times 10^{15} M_{\odot}$ with a typical mass spacing of $\sim 4 \times 10^{13} M_{\odot}$) were sampled for each viewing angle. These results demonstrate that the observed velocity distribution in A665 is consistent with the velocity distribution expected from the major merger of two similar sized subclusters, close to or after the time of core-crossing, with the exact epoch depending on the mass ratio and viewing geometry.

Another view of the mass of A665 inferred from the allowed merger models is shown in Figure 7. Here we plot the mass within r_{500} , which is the radius at which the cluster density is equal to 500 times the critical density. Evrard et al. (1996) have shown from numerical simulations of cluster evolution that r_{500} can be expressed as a power law of the gas temperature. For A665 with a global temperature of 8.3 keV, we compute a value of $r_{500} = 1.5$ Mpc from this relation. According to Fig. 7 the inferred total cluster mass within this radius based on galaxy dynamics is in the range $1.6 \times 10^{15} M_{\odot}$ to $2.4 \times 10^{15} M_{\odot}$. These estimates are consistent with the total mass ($1.7 \times 10^{15} M_{\odot}$) predicted by the scaling relations proposed by Evrard et al. (1996). However, they are somewhat in excess of the mass estimate ($0.9 - 1.5 \times 10^{15} M_{\odot}$) from an X-ray analysis by Hughes & Tanaka (1992) under the typical assumptions of hydrostatic equilibrium and spherical symmetry. Numerical simulations of cluster mergers and evolution (e.g., Evrard et al. 1996, Roettiger et al. 1996) show that one can overestimate or underestimate the actual mass of a merging cluster by factors of 2 if one assumes hydrostatic equilibrium and isothermal β -models. The exact difference between the true cluster mass and the inferred mass from X-ray analysis depends on the geometry, epoch, and other gas parameters (e.g., temperature, core radius, β) of the merging clusters. Thus, it is not surprising that our mass estimates from galaxy dynamics are not in perfect agreement with the X-ray-derived mass.

Looking at the results of the 1:1 merger in more detail, we find that the K-S test rejects mergers at epochs slightly earlier than -0.5 Gyr because the velocity distributions tend to be either bimodal or very broad (depending on the viewing angle) and therefore incompatible with the data. On the other hand, mergers at even earlier epochs (before -1 Gyr) or at late epochs (after 1 Gyr) are rejected because the K-S test finds the velocity distributions to be more symmetric and/or wider than our data. Thus, this test is more sensitive to the marginal non-Gaussianity of our data than the generic statistical tests that we used before (see section 3.1). The situation for the 1:2 mass ratio mergers is somewhat different. The velocity distributions produced by these simulations do allow a larger range of models due to the smaller effect that the subcluster has on the overall shape of the velocity distribution. In other words, our analysis is consistent with two similar-size clusters caught in the middle of a merger or a larger system being affected by a smaller subcluster. Note that there are no acceptable models for earlier epochs (more than 1 Gyr before core-crossing) that would correspond to relaxed clusters seen in projection if viewed along

the merger axis since such models would display spatial distributions of galaxies that would be clearly bimodal and therefore inconsistent with the data.

Our optical velocity data showed marginal evidence for a difference in the mean velocity and velocity dispersion with position (Table 3). We have used this information in an attempt to further discriminate among allowed models. From the N-body models we extracted the line-of-sight velocities of 54 objects in the inner 750 kpc (corresponding to our central sample) and 23 objects from within an annular region from 750 kpc to 2 Mpc (corresponding to the outer sample). Here we have estimated 2 Mpc to be roughly the outermost radial extent of OHFH’s study. For each merger epoch, mass ratio, and viewing angle we calculated the mean velocities and dispersions in the two extraction regions. Sampling errors were taken into account by averaging the values obtained from 100 independent random extractions. The 1:1 merger does not show any evidence at all for a gradient in the mean velocity, although there is evidence for a velocity dispersion gradient especially for epochs close to core-crossing. Specifically, the velocity dispersions from the two regions differ by approximately $300\text{--}600\text{ km s}^{-1}$ with the maximum difference occurring at core crossing. The situation is much different for the 1:2 merger. In this case there is evidence for a gradient in both mean velocity and velocity dispersion. For epochs between -1 Gyr and 2 Gyr from core crossing, the mean velocities differ by $200\text{--}400\text{ km s}^{-1}$ and the velocity dispersions differ by $400\text{--}800\text{ km s}^{-1}$ for the inner and outer galaxy samples. These values are comparable to our measured values. Therefore, of all the models considered in our analysis, the 1:2 merger seen close to the time of core crossing appears to be the most consistent with our galaxy velocity data.

Although detailed modeling of the properties of the X-ray emission arising from a merger of this type is beyond the scope of our work, the properties of the merger inferred from the galaxy velocities (i.e., small mass ratio, close to core-crossing) are qualitatively consistent with the distorted morphology of the X-ray emission (Roettiger et al. 1996). We await upcoming X-ray spectral images from *Chandra* that will allow us to further investigate the properties of the hot gas in A665 and probe the evolutionary state of this complex merging system in greater detail.

5. SUMMARY AND CONCLUSIONS

We measured new R-band optical magnitudes for 147 galaxy candidates in the vicinity of the rich galaxy cluster A665. A total of 89 of these candidates were observed at the MMT; good signal-to-noise spectra that resulted in the identification and determination of recessional velocities were obtained for 55 galaxies. Combining with data in the literature results in a total of 77 known cluster member galaxies in A665. We concentrate our study of the cluster’s kinematics on the subsample of 54 galaxies within the inner $4\frac{1}{2}$ (750 kpc) central region of the cluster.

We find, at most, marginal evidence for kinematic structure and non-Gaussianity in the velocity data of the central subsample of galaxies. In addition for these galaxies there is only weak evidence for 3-D spatial and kinematical clustering as detected by the Dressler-Schectman test.

Comparison of the central subsample to the sample of cluster members beyond $4/5$ of the center, shows marginal ($\sim 2\sigma$) evidence for a drop in both the mean velocity and velocity dispersion. Taken at face value the optical velocity data therefore appear consistent with a massive relaxed cluster, exhibiting only subtle signs of substructure. Others have pointed out that the spatial distribution of galaxies shows some evidence for substructure.

Our deep *ROSAT* HRI observation of A665 reveals strong signatures of substructure in the spatial distribution of the X-ray emitting gas that are consistent with PSPC observations (Hughes & Birkinshaw 2000). We have measured centroid shifts, ellipticity variations, and the rotation (or twist) of elliptical isophotes as a function of distance from the cluster center. These indicate recent merger activity in the cluster.

In order to reconcile these two apparently conflicting views of the cluster’s evolutionary state, we have undertaken simple N-body simulations of head-on cluster mergers. We find that the velocity distributions produced by the merger of two subclusters with mass ratios of 1:1 or 1:2 near the time of core-crossing provide an acceptable match to the observed velocity distribution of the central subsample for a range of reasonable viewing geometries. In addition, near the epoch of core-crossing the 1:2 merger produces a radial gradient in mean velocity and dispersion that also agrees with our measurements. A major merger of this type is at least qualitatively consistent with the distorted X-ray morphology of A665.

Major new insights into the nature of this cluster and the process of cluster formation in general should be forthcoming with the data expected from the new generation of X-ray missions recently launched. *Chandra* and *XMM* will provide detailed measurements of the cluster’s gas temperature and density that are sure to provide excellent views of shocks and other plasma processes in the hot gas. Furthermore, our simulations indicate that increasing to ~ 250 the number of cluster member galaxies in A665 with good redshift measurements would allow us to observe directly the effects of the merger on the galaxy velocity distribution. Each of these techniques yields a different view of the ongoing merger in A665 and thus merits follow-up.

This work was partially supported by a PPARC grant to MB and NASA grants NAG5-3432, NAG5-4794, and NAG5-6420 to JPH. We would like to express our thanks to Neil Trentham who kindly provided us with his A665 optical images and to Tad Pryor for insightful comments about the work. We also thank the CfA time allocation committee for their patience and generosity in awarding us MMT observing time over the many years this project took. Support from Monique Arnaud and the hospitality of the XMM group at the Service d’Astrophysique of the CEA-Saclay is also gratefully acknowledged by JPH.

REFERENCES

- Abell, G. O. 1958, ApJS, 3, 211
- Beers, T. C., Gebhardt, K., Forman, W., Huchra, J. P., & Jones, C. 1991, AJ, 102, 1581
- Bird, C., & Beers, T. 1993, ApJ, 105, 1596
- Binney, J. & Tremaine, S. 1987, Galactic Dynamics, Princeton University Press
- Birkinshaw, M. 1979, MNRAS, 187, 847
- Birkinshaw, M., Hughes, J. P., & Arnaud, K. A. 1991, ApJ, 379, 466
- Buote, D. A., & Tsai, J. C. 1996, ApJ, 458, 27
- D’Agostino, R. B. 1986, in Goodness of Fit Techniques, eds., R. B. D’Agostino & M. A. Stephens (New York: Marcel Dekker), 367
- Danese, L., De Zotti, G., & di Tullio, G. 1980, A&A, 49, 137
- David, L. P., Harnden, F. R., Kearns, K. E., Zombeck, M. V., Harris, D. E., Prestwich, A., Primini, F. A., Silverman, J. D., & Snowden, S. L. 1998, The *ROSAT* High Resolution Imager (HRI) Calibration Report.
- de Vaucoulers, G., de Vaucoulers, A., Corwin, Jr., H. G., Buta, R. J., Paturel, G., & Fouque, P. 1991, Third Reference Catalogue of Bright Galaxies (New York: Springer-Verlag)
- Dressler, A., & Shectman, S. A. 1988, AJ, 95, 985
- Edge, A. C., & Stewart, G. C. 1991, MNRAS, 252, 414
- Evrard, A. E. 1990, ApJ, 363, 349
- Evrard, A. E., Metzler, C. A., & Navarro, J. F. 1996, ApJ, 469, 494
- Fabricant, D. G., McClintock, J. E., & Bautz, M. W. 1991, ApJ, 381, 33
- Garilli, B., Bottini, D., Maccagni, D., Carrasco, L., & Recillas, E. 1996, ApJS, 105, 191
- Geary, J., Huchra, J., & Latham, D. 1986, SPIE Proc. 627, 509
- Geller, M. J., & Beers, T. C. 1982, PASP, 94, 421
- Girardi, M., Fadda, D., Giuricin, G., Madirossian, F., Mezzetti, M., & Biviano, A. 1996, ApJ, 457, 61
- Gunn, J. E. 1978, in Observational Cosmology, eds., A. Maeder, L. Martinet, & G. Tammann (Sauverny: Geneva Observatory), 1

- Hernquist, L. 1987, ApJS, 64, 715
- Huang, Z., & Sarazin, C. L. 1997, ApJ, 461, 622
- Hughes, J. P. 1989, ApJ, 337, 21
- Hughes, J. P., & Birkinshaw, M. 1994, in *The Soft X-Ray Cosmos*, AIP Conf. Proc. 313, eds., E. M. Schlegel & R. Petre (AIP: New York), 378.
- Hughes, J. P., & Birkinshaw, M. 2000, in preparation
- Hughes, J. P., & Tanaka, Y. 1992, ApJ, 398, 62.
- Jedrzejewski, R. I. 1987, MNRAS, 226, 747
- Kalloglyan, A. T., Nanni, D., and Viganato, A. 1990, *Astrophysics* (tr. *Astrofizika*), 31, 672
- King, I. R. 1966, AJ, 61, 74
- Landolt, A. U. 1992, AJ, 104, 340
- Markevitch, M. 1996, ApJ, L1, 465
- Moffet, A. T., & Birkinshaw, M. 1989, AJ, 98, 1148
- Mohr, J. J., Mathiesen, B., & Evrard, A., ApJ, 517, 627
- Oegerle, W. R., Fitchett, M. J., Hill, J. M., & Hintzen P. 1991, ApJ, 376, 46 (OFHF)
- Pearce, F. R., Thomas, P. A., & Couchman, H. M. P. 1994, MNRAS, 268, 953
- Pinkney, J., Roettiger, K., Burns, J. O., & Bird, C. 1996, ApJS, 104, 1
- Richstone, D., Loeb, A. & Turner, E. L. 1992, ApJ, 393, 477
- Roettiger, K., Burns, J. O., Loken, C. 1996, ApJ, 473, 651
- Schindler, S., & Müller, E. 1993, A&A, 272, 137
- Schmidt, G., Weymann, R., & Foltz, C. 1989, PASP, 101, 713
- Sunyaev, R. A. & Zel'dovich, Ya. B. 1972, *Comm. Astrophys. Sp. Phys.*, 4, 173
- Tonry, J. & Davies, M. 1979, AJ, 84, 1511
- Trentham, N. 1998, MNRAS, 295, 360
- White, D. A. & Fabian, A. C. 1995, MNRAS, 273, 72
- Wilson, G., Smail, I., Ellis, R. S., Couch, W. J. 1997, MNRAS, 284, 915

Yahil, A., & Vidal, N. V. 1977, ApJ, 214, 347

Zabludoff, A. I., Geller, M. J., Huchra, J. P., & Ramella, M. 1993, AJ, 106, 1301

Fig. 1.— Overlay of X-ray surface brightness contours on an optical R band grayscale image of A665. The contour levels are at values of 6, 18, 30, 48, 66, 72, 102, 120, 138, and 180×10^{-4} HRI counts $\text{s}^{-1} \text{ arcmin}^{-2}$. The *ROSAT* HRI X-ray image has been adaptively smoothed and clearly shows a cluster with asymmetric isophotes.

Fig. 2.— Velocity histogram of the 54 cluster member galaxies located within 750 kpc of the center of A665. All velocities have been corrected to the cluster reference frame. The bin size is 1000 km s^{-1} .

Fig. 3.— Contours of *ROSAT* HRI X-ray surface brightness superposed with the results of the Dressler-Schectman 3-D test for substructure. The contours are identical to Fig. 1 except that the central contour is omitted for clarity. Each circle represents the position of a galaxy and the size of the circle is proportional to the exponential of the deviation between the local and global mean velocities and velocity dispersions.

Fig. 4.— X-ray surface brightness contours overlaid on a grayscale map of the galaxy surface density for secure cluster members in A665. The contours are identical to those in Fig. 1. Both maps have been adaptively smoothed. Note the offset in peak density between the two distributions and the NW-SE elongation of each.

Fig. 5.— Elliptical isophotal analysis of the *ROSAT* HRI X-ray image. The four panels (starting at top left and proceeding counterclockwise) show the ellipticity (b/a is the axis ratio), position angle of the major axis (measured positive counterclockwise from north), centroid shift in declination and centroid shift in right ascension. Note the large centroid shift apparent in the bottom panels.

Fig. 6.— Allowed merger models plotted as a function of main cluster mass and time since merger, based on comparing the line-of-sight velocity distributions from the 54 galaxies near the center with the modeled distributions. Those models with a K-S probability greater than 90% are shown; many other possible models were rejected. The top panel corresponds to a mass ratio of 1 to 2 between the merging components, while the bottom panel corresponds to the merger of equal mass subclusters. We have indicated how the results depend on viewing angle for three different values (where 0° corresponds to viewing along the merger axis). In both panels the plus symbol corresponds to a 90° viewing angle, the cross corresponds to a 45° viewing angle, and the triangle corresponds to a 30° viewing angle.

Fig. 7.— Same as Fig. 6 except that the allowed merger models are plotted as a function of total cluster mass within the virial radius ($r_{500} = 1.5 \text{ Mpc}$).

Table 1. Observation Log

Dates of Observation	Technique	Instrument and Grating
4-9 April 1986	slitlets	FOGS 400 lines mm ⁻¹
20 January 1988	slitlets	FOGS 400 lines mm ⁻¹
5-6 January 1989	aperture plates	FOGS 300 lines mm ⁻¹
3-5 June 1989	aperture plates	Red Channel 270 lines mm ⁻¹
1 January 1990	aperture plates	Red Channel 270 lines mm ⁻¹
30-31 March 1990	aperture plates	Red Channel 270 lines mm ⁻¹
19-20 January 1991	aperture plates	Red Channel 270 lines mm ⁻¹

Table 2. Galaxies in the A665 field

Galaxy ID	RA(2000)	DEC(2000)	Heliocentric Velocity	error	TDR value	R magnitude	comments
1	8 30 34.5	65 51 50.0	54645	96	9.7	17.8	OFHF # 231
2	8 30 36.0	65 52 36.9	56477	117	3.7	17.5	OFHF # 235
3	8 30 37.1	65 49 27.8	56895	98	7.4	19.2	
4	8 30 37.7	65 50 58.9	55001	113	3.9	19.8	
5	8 30 38.1	65 51 39.8	57564	159	6.5	18.1	
6	8 30 38.8	65 52 50.6	56874	112	5.3	19.3	
7	8 30 39.1	65 49 49.0	54987	113	5.0	20.1	
8	8 30 39.1	65 49 16.7	54000	101	6.8	19.2	
9	8 30 40.2	65 50 25.3	56223	150	...	18.7	BLG
10	8 30 40.3	65 48 27.1	56400	93	12.7	18.1	
11	8 30 41.5	65 50 46.1	51186	150	...	19.1	BLG
12	8 30 42.4	65 50 34.6	51030	101	6.5	17.4	OFHF # 225
13	8 30 43.9	65 51 28.7	76726	111	4.3	18.9	BG
14	8 30 46.3	65 51 12.4	70969	97	4.7	20.3	BG
15	8 30 48.2	65 52 33.1	54477	115	8.2	18.6	
16	8 30 49.0	65 50 00.3	52381	108	5.2	18.5	
17	8 30 49.7	65 48 52.2	55987	112	4.4	20.1	
18	8 30 50.4	65 51 06.7	51728	118	4.7	18.6	
19	8 30 51.4	65 48 38.7	53033	104	4.9	19.1	
20	8 30 52.7	65 49 25.6	82649	109	3.7	19.1	BG
21	8 30 52.8	65 48 48.8	57751	112	4.7	18.3	
22	8 30 53.6	65 50 42.7	55998	103	7.6	18.2	
23	8 30 53.9	65 51 23.1	56261	97	8.6	18.3	
24	8 30 54.5	65 51 24.4	56023	102	7.9	18.3	
25	8 30 54.9	65 52 16.8	53773	101	9.0	17.7	
26	8 30 55.4	65 50 05.8	56745	91	11.8	18.6	
27	8 30 55.5	65 50 40.8	53850	98	11.4	19.0	
28	8 30 55.6	65 51 37.4	54583	101	6.1	19.7	
29	8 30 55.8	65 49 00.7	56617	100	7.3	18.5	
30	8 30 56.0	65 51 02.4	55729	112	4.4	19.3	
31	8 30 56.2	65 49 46.4	56121	95	10.9	18.3	
32	8 30 56.2	65 49 11.4	55361	94	11.1	18.2	
33	8 30 56.7	65 50 57.7	57783	99	6.7	19.8	
34	8 30 57.6	65 50 29.6	55015	90	16.7	17.2	BCM, OFHF # 201
35	8 30 58.5	65 51 16.2	56502	106	7.2	19.7	
36	8 30 58.7	65 48 47.7	55812	113	5.1	20.0	
37	8 30 59.0	65 50 22.9	53306	94	12.8	17.5	
38	8 30 59.7	65 52 12.9	54722	102	6.5	20.2	
39	8 31 00.6	65 50 22.0	54315	108	4.5	20.7	
40	8 31 01.1	65 50 42.8	57303	107	4.6	19.4	
41	8 31 02.3	65 49 36.6	54785	101	7.8	18.9	
42	8 31 03.5	65 50 47.5	53476	93	14.1	17.4	OFHF # 224
43	8 31 05.4	65 51 04.1	50874	91	13.8	18.2	
44	8 31 05.6	65 48 46.5	44333	138	4.9	18.0	FG
45	8 31 07.9	65 49 24.2	54959	95	8.9	18.8	
46	8 31 10.7	65 49 16.5	56906	98	6.8	18.1	OFHF # 218
47	8 31 11.1	65 51 46.8	53212	95	5.9	19.9	
48	8 31 11.6	65 49 27.7	54243	106	6.9	18.9	
49	8 31 12.3	65 52 42.4	53281	105	6.0	18.0	OFHF # 234
50	8 31 13.2	65 49 35.4	56897	98	6.8	18.1	
51	8 31 14.2	65 50 45.5	53624	123	7.3	18.5	
52	8 31 16.3	65 51 36.2	55909	114	5.3	19.4	

Table 2—Continued

Galaxy ID	RA(2000)	DEC(2000)	Heliocentric Velocity	error	TDR value	R magnitude	comments
53	8 31 19.0	65 51 06.6	54356	129	4.4	19.8	
54	8 31 22.5	65 49 13.1	54226	116	6.0	18.6	
55	8 31 23.3	65 52 33.1	54307	114	5.6	19.2	
56	8 30 35.8	65 52 32.3	18.3	
57	8 30 36.1	65 54 07.7	17.9	
58	8 30 36.1	65 49 50.7	19.7	
58	8 30 37.4	65 52 22.8	19.5	o
60	8 30 38.4	65 53 33.0	17.9	
61	8 30 39.4	65 50 35.1	19.3	o
62	8 30 41.7	65 52 17.6	20.3	
63	8 30 42.1	65 49 07.9	20.3	o
64	8 30 43.0	65 49 45.6	20.6	
65	8 30 43.1	65 50 18.4	12.2	gsc, o
66	8 30 43.5	65 50 43.8	18.2	OFHF # 227, BG, o
67	8 30 43.9	65 48 01.3	19.7	o
68	8 30 44.0	65 50 34.3	20.4	o
69	8 30 44.3	65 50 40.8	19.4	
70	8 30 44.6	65 52 12.5	19.9	
71	8 30 44.9	65 51 55.1	19.4	o
72	8 30 45.4	65 48 25.1	18.8	
73	8 30 45.4	65 50 42.7	20.6	
74	8 30 46.4	65 52 54.7	20.3	o
75	8 30 46.7	65 49 47.6	19.4	
76	8 30 47.4	65 50 59.9	15.9	ps
77	8 30 47.7	65 49 27.4	20.7	
78	8 30 48.3	65 49 57.9	19.1	
79	8 30 49.2	65 50 50.6	14.5	gsc
80	8 30 49.5	65 47 57.1	19.8	o
81	8 30 50.7	65 48 34.6	20.0	o
82	8 30 50.9	65 51 23.1	15.9	ps
83	8 30 51.0	65 49 28.2	18.0	s,o
84	8 30 51.3	65 51 12.1	18.3	
85	8 30 51.3	65 51 30.4	19.8	o
86	8 30 51.9	65 52 25.7	18.0	o
87	8 30 52.2	65 49 20.4	20.2	
88	8 30 52.4	65 51 03.2	20.2	o
89	8 30 52.5	65 48 58.7	20.3	
90	8 30 52.7	65 52 21.3	19.4	o
91	8 30 54.7	65 50 22.8	20.0	
92	8 30 54.7	65 49 24.1	19.5	o
93	8 30 55.0	65 52 08.4	18.6	
94	8 30 55.8	65 50 49.4	20.6	
95	8 30 56.0	65 52 04.6	18.6	
96	8 30 57.0	65 49 48.6	20.1	o
97	8 30 57.8	65 50 17.3	19.3	
98	8 30 58.2	65 52 26.5	20.0	
99	8 30 58.4	65 50 17.2	20.2	
100	8 30 58.7	65 50 07.0	20.5	
101	8 30 58.7	65 48 02.3	19.6	
102	8 30 58.9	65 50 42.6	19.7	
103	8 30 59.2	65 50 52.2	18.1	ps, o
104	8 30 59.5	65 50 20.6	17.8	

Table 2—Continued

Galaxy ID	RA(2000)	DEC(2000)	Heliocentric Velocity	error	TDR value	R magnitude	comments
105	8 30 59.6	65 50 57.2	19.5	o
106	8 30 59.7	65 49 34.6	20.5	
107	8 30 59.9	65 50 47.8	20.0	o
108	8 31 00.3	65 51 47.9	14.9	gsc
109	8 31 00.6	65 48 59.2	19.4	o
110	8 31 00.6	65 51 37.6	19.6	
111	8 31 00.8	65 48 41.3	20.0	o
112	8 31 01.5	65 48 08.7	20.2	
113	8 31 03.1	65 50 02.4	19.9	
114	8 31 03.2	65 49 55.8	17.6	
115	8 31 03.4	65 48 51.7	20.1	
116	8 31 04.1	65 50 09.1	19.0	
117	8 31 05.2	65 47 52.9	19.4	o
118	8 31 05.6	65 51 56.5	20.7	
119	8 31 05.6	65 51 08.9	19.2	o
120	8 31 05.6	65 50 43.6	19.9	pb, o
121	8 31 06.4	65 48 14.7	19.9	
122	8 31 06.6	65 49 38.4	20.1	
123	8 31 06.9	65 50 17.8	16.9	ps
124	8 31 07.2	65 49 19.4	18.4	o
125	8 31 07.3	65 51 35.1	20.4	
126	8 31 07.9	65 50 43.0	19.5	
127	8 31 07.9	65 50 05.7	20.0	o
128	8 31 08.0	65 49 35.7	19.4	o
129	8 31 08.3	65 51 43.5	19.3	o
130	8 31 09.9	65 48 40.6	19.8	
131	8 31 10.1	65 48 11.9	17.0	ps
132	8 31 10.4	65 47 48.3	20.2	
133	8 31 11.0	65 51 41.3	19.8	o
134	8 31 11.2	65 49 52.5	20.6	
135	8 31 13.8	65 49 36.8	18.1	o
136	8 31 16.2	65 49 42.0	20.8	
137	8 31 16.2	65 49 03.7	17.9	
138	8 31 16.4	65 50 26.9	18.1	
139	8 31 18.6	65 52 10.3	18.1	
140	8 31 18.6	65 48 38.4	20.0	
141	8 31 19.1	65 50 01.6	19.2	
142	8 31 19.3	65 52 51.4	20.0	o
143	8 31 19.5	65 49 28.3	19.5	o
144	8 31 20.8	65 49 47.6	20.1	
145	8 31 22.6	65 51 31.7	18.0	
146	8 31 23.4	65 48 19.4	20.6	
147	8 31 23.7	65 52 20.9	20.3	

NOTES

BCM: brightest cluster member

OFHF: galaxy also in Oegerle et al. 1991 sample

BLG: galaxy with strong Balmer absorption lines

BG: confirmed background galaxy

FG: confirmed foreground galaxy

o: object was observed spectroscopically but the crosscorrelation gave a low TDR value.

gsc: Guide Star Catalog Star. The magnitude for # 65 is from the GSC.

pb: We determine that this object is a possible background galaxy. Its crosscorrelation yielded a velocity $\sim 77,000$ km s⁻¹ with a low TDR value of 3.4.

s: stellar spectrum

Table 3. Velocity Data

Sample	Number of Galaxies	Redshift	σ_{LOS} (km s ⁻¹)
All Galaxies	77	$0.18285^{+0.00045}_{-0.00064}$	1390^{+120}_{-110}
Our Sample	51	$0.18373^{+0.00067}_{-0.00102}$	1500^{+190}_{-110}
OHFH	33	$0.18170^{+0.00094}_{-0.00074}$	1230^{+250}_{-140}
Central Galaxies ($R < 4'.5$)	54	$0.18347^{+0.00082}_{-0.00084}$	1430^{+170}_{-140}
Outer Galaxies ($R > 4'.5$)	23	$0.18110^{+0.00072}_{-0.00064}$	1050^{+270}_{-190}

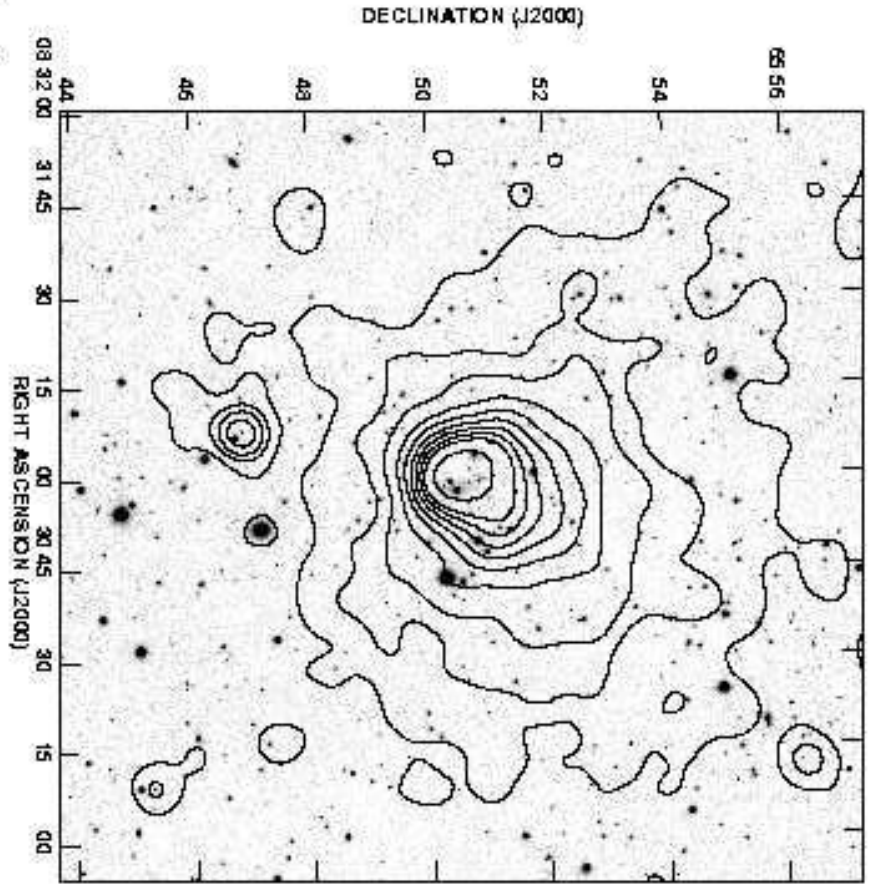


Figure 1.

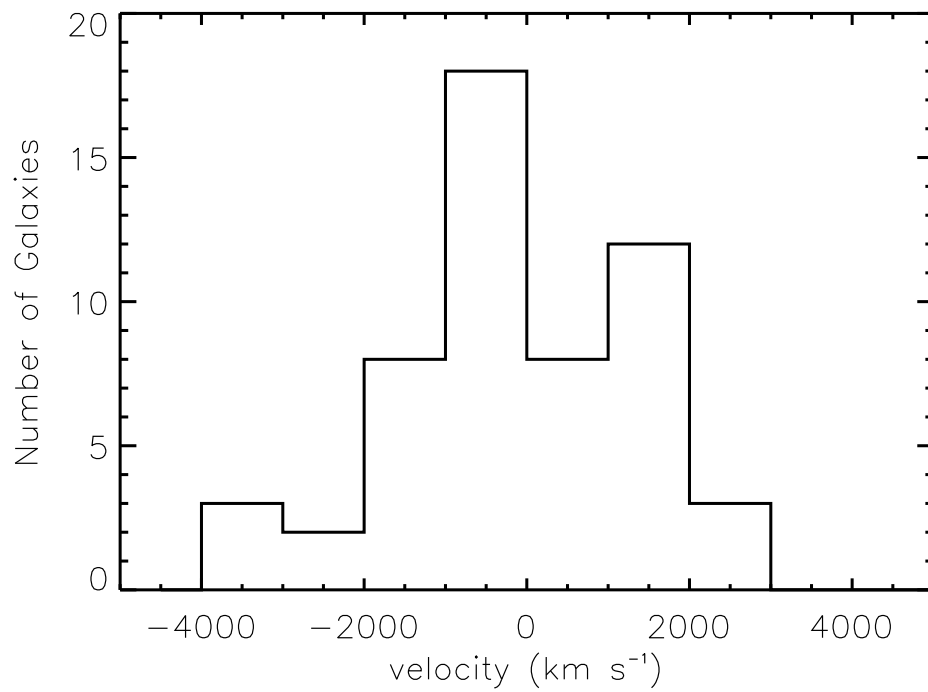


Figure 2.

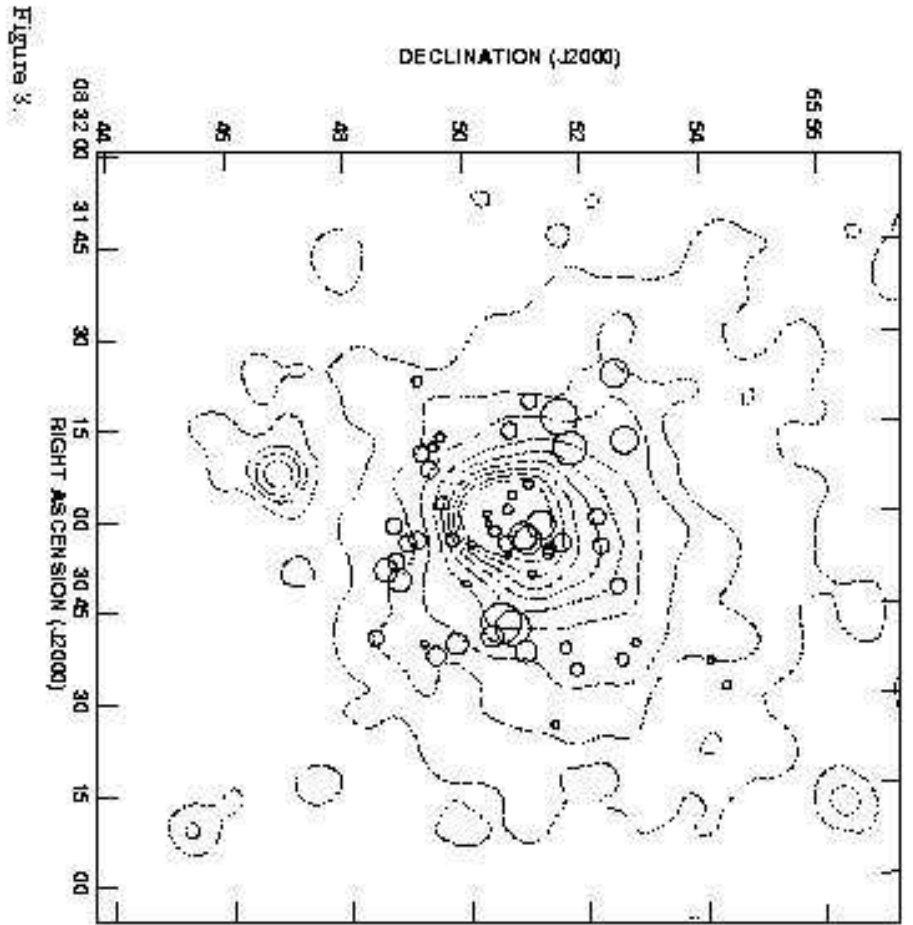


Figure 3.

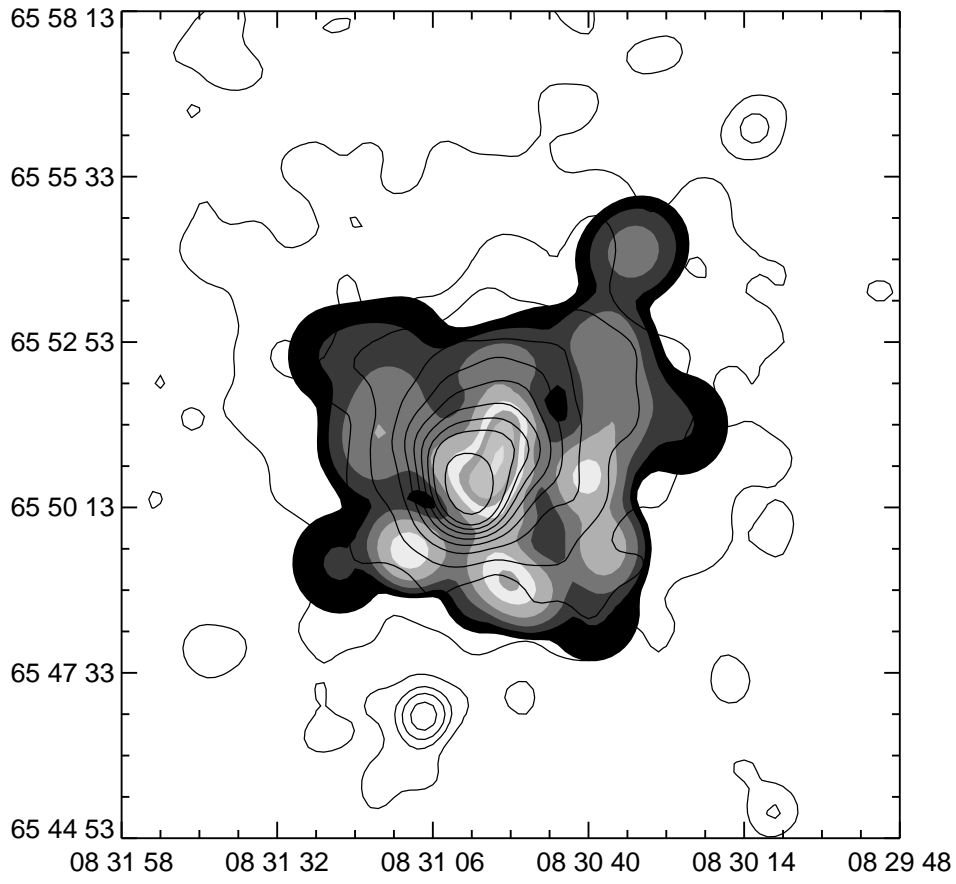


Figure 4.

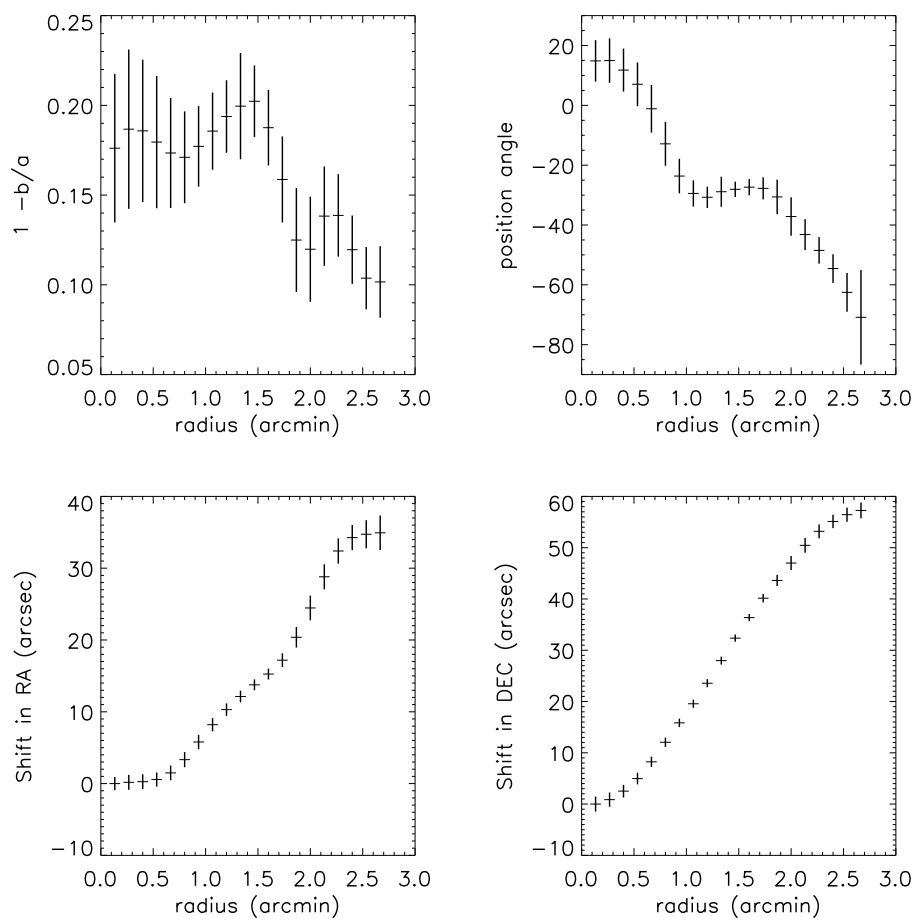


Figure 5.

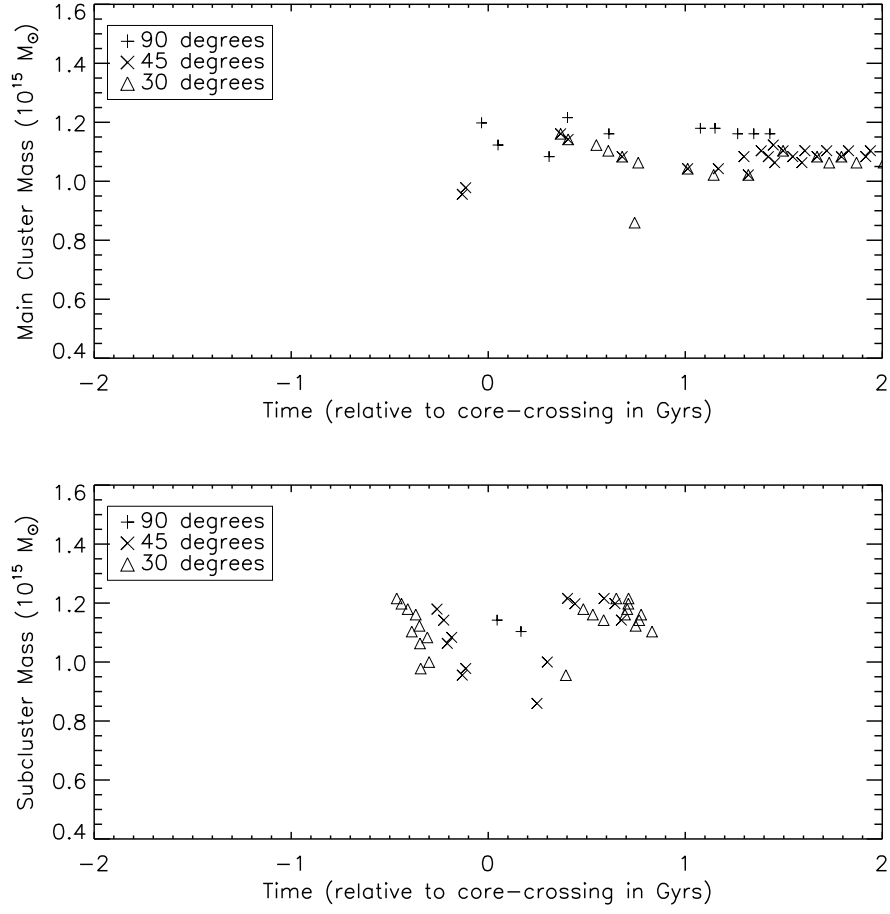


Figure 6.

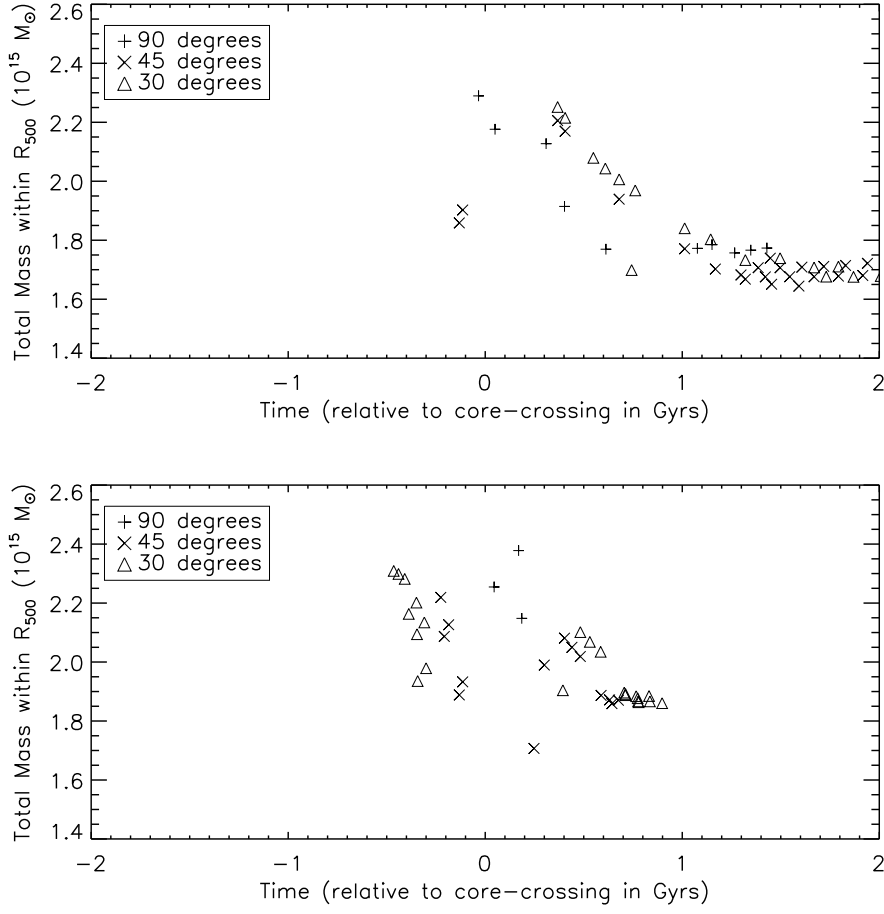


Figure 7.

This figure "f1.jpg" is available in "jpg" format from:

<http://arxiv.org/ps/astro-ph/0004263v1>

This figure "f3.jpg" is available in "jpg" format from:

<http://arxiv.org/ps/astro-ph/0004263v1>